ACS APPLIED MATERIALS & INTERFACES

Research Article

www.acsami.org

Hydrothermal Synthesis of Mo-Doped VO_2/TiO_2 Composite Nanocrystals with Enhanced Thermochromic Performance

Dengbing Li,[†] Ming Li,[†] Jing Pan,[†] Yuanyuan Luo,[†] Hao Wu,[†] Yunxia Zhang,[†] and Guanghai Li*[,†,‡]

[†]Key Laboratory of Materials Physics, Anhui Key Laboratory of Nanomaterials and Nanotechnology, Institute of Solid State Physics, Chinese Academy of Sciences, Hefei 230031, P. R. China

[‡]University of Science and Technology of China, Hefei 230026, P. R. China

Supporting Information

ABSTRACT: This paper reports a one-step TiO_2 seed-assistant hydrothermal synthesis of Mo-doped VO_2(M)/TiO_2 composite nanocrystals. It was found that excess Mo doping can promote formation of the VO_2(M) phase, and rutile TiO_2 seed is beneficial to morphology control, size reduction, and infrared modulation of Mo-doped VO_2(M) nanocrystals. The Mo-doped VO_2 nanocrystals epitaxially grow on TiO_2 seeds and have a quasi-spherical shape with size down to 20 nm and a nearly 35% infrared modulation near room temperature. The findings of this work demonstrate important progress in the near-room-temperature thermochromic performance of VO_2(M) nanomaterials, which will find potential application in constructing VO_2(M) nanocrystal-based smart window coatings.

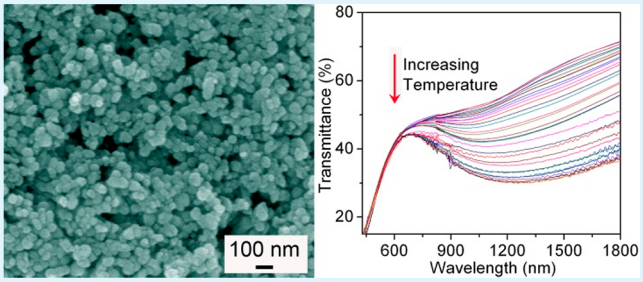

KEYWORDS: *VO_2 nanocrystals, hydrothermal, rutile TiO_2 seed, phase transition temperature, thermochromic performance*

1. INTRODUCTION

Monoclinic phase vanadium dioxide [VO_2(M)] is a promising material for thermochromic smart windows because of its reversible phase transition between monoclinic and rutile phases [VO_2(M) ↔ VO_2(R)] at T_c ~338 K, leading to dramatically changed electrical and optical properties.[1,2] VO_2(M) is a metallic material with high infrared reflection when the temperature is above T_c and becomes a semiconductor with a reasonable infrared transmission when the temperature is below T_c.[3−5] The modulation of T_c to room temperature is essential for many practical applications not limited to smart windows. A number of approaches have been reported for the reduction of T_c, and among them, doping of VO_2(M) with metal ions (e.g., W^{6+}, Mo^{6+}, Ta^{5+}, Nb^{5+}, and Ru^{4+}) is a commonly used strategy but often leads to a decreased thermochromic performance.[6]

Hydrothermal synthesis is a commonly used method, and it has been demonstrated that if the hydrothermal reaction temperature is not high enough and/or the reaction time is not long enough, the VO_2(B) phase instead of the VO_2(M) phase will be obtained. Pure single-crystal VO_2(R) powders have been synthesized by the hydrothermal treatment of V_2O_5 and oxalic acid at 240 °C for 7 days.[7] VO_2(R) nanorods have also been fabricated using the same reaction at 260 °C for at least 16 h.[8] VO_2(M) micro- and nanocrystals were prepared using N_2H_4 as a reducing agent.[9] Pure and W-doped VO_2(M) nanobelts were obtained using V_2O_4 and a mixture of V_2O_5, $H_2C_2O_4$ (oxalic acid), and H_2WO_4.[10,11] VO_2(M) powders have been synthesized by either an ultrafast solid-state reaction of VOOH or direct combustion of a $VO(acac)_2$ ethanolic solution.[12,13] VO_2(M) ultrathin nanosheets were successfully fabricated by chemical lithiation and exfoliation−deintercalation using VO_2(M) bulk.[14] Owing to the high temperature and long reaction time, overgrowth of VO_2(M) is a common issue in the hydrothermal synthesis.

Rutile TiO_2 has the same structure as VO_2(R) with approximate lattice parameters, and the crystal structure of VO_2 is sensitive to under- and/or overcoated materials, which promises that the rutile TiO_2 nanocrystal can be used as a seed to assist the nucleation and growth of rutile VO_2 with nanostructure. Moreover, the VO_2(M)/TiO_2 composite has its own advantages in not only increasing the luminous transmittance but also modifying the infrared modulation ability.[15−17] The reported fabrication methods of the VO_2(M)/TiO_2 composite are limited to sol−gel, chemical, and/or physical vapor deposition,[15−17] which cannot meet the requirements for the production of large-area VO_2 thermochromic windows because of technical and cost problems. A nanoparticle-based solution coating is an alternative way to fabricate the thermochromic film because of its simple coating system, flexibility for substrate selection, ease of large-scale production, and low cost.[18]

In this paper, we report a one-step TiO_2 seed-assistant hydrothermal synthesis of Mo-doped VO_2(M)/TiO_2 composite nanocrystals. It was found that the size and phase transition temperature of the composite nanocrystals can be regulated by

Received: January 8, 2014
Accepted: April 15, 2014
Published: April 15, 2014

   dx.doi.org/10.1021/am500135d | ACS Appl. Mater. Interfaces 2014, 6, 6555−6561

the content of TiO_2 seed and a good near-room-temperature thermochromic performance has been realized.

2. EXPERIMENTAL SECTION

2.1. Materials. Oxalic acid ($H_2C_2O_4{\cdot}2H_2O$, purchased from Chinese Sinopharm Chemical Reagent Co., Ltd., Shanghai, China), vanadium pentoxide (V_2O_5, purchased from Research Institute of Tianjin Guangfu Fine Chemical Research Institute, Beijing, China), and molybdic acid (H_2MoO_4, purchased from Shanghai Senhao Fine Chemicals Co. Ltd., Shanghai, China) were used without purification. Rutile TiO_2 nanoparticles (with sizes of 11−20 nm; purchased from Hangzhou Wan Jing New Material Co., Ltd., Zhejiang, China) were used as received.

2.2. Synthesis of Mo-Doped VO_2(M) Nanorods. For a typical synthesis procedure, an appropriate amount of oxalic acid was first dissolved in 35 mL of deionized water with constant stirring in a 50 mL Teflon cup followed by the addition of proportional quantities of oxalic acid, vanadium pentoxide (the molar ratio of oxalic acid and vanadium pentoxide is 1−2:1), and molybdic acid. The resultant solution was stirred for 1 h and then heated in a sealed autoclave with a stainless steel shell at 220 °C for 2 days. The black precipitate was collected after cooling naturally to room temperature, washed three times using deionized water and alcohol alternatively, and then dried at 60 °C for 12 h. The pure VO_2(B) nanopowders were synthesized using the same procedures except the addition of molybdic acid.

2.3. Synthesis of Mo-Doped VO_2/TiO_2 Composite Nanocrystals. Similar to the above procedures, after stirring for 1 h, a certain amount of rutile TiO_2 nanocrystals with average sizes of about 15 nm was added to the solution and stirred for another 2 h; the resultant solution was heated in a sealed autoclave with a stainless steel shell at 220 °C for 2 days, and the rest of the procedures are the same as those mentioned above. After mixing with 5 wt % poly(vinylpyrrolidone) in alcohol, the Mo-doped VO_2(M) and VO_2/TiO_2 composite nanocrystal films on a glass substrate were obtained by spin coating at a speed of 5000 rpm.

2.4. Characterizations. The microstructure of the products was determined by X-ray diffraction (XRD; Philips X'Pert Pro MPD and Cu Kα radiation at 1.54056 Å), field-emission scanning electron microscopy (FESEM; Sirion 200 operating with an accelerating voltage of 10 kV), and transmission electron microscopy (TEM; JEOL model 2010). The valence state and chemical composition were studied by X-ray photoelectron spectroscopy (XPS; PerkinElmer PHI-5600ci). The phase transition behavior was analyzed by differential scanning calorimetry (DSC; Netzsch DSC-4000) at a temperature ramp rate of 10 °C/min within the −20 to +100 °C range in a flowing nitrogen atmosphere. Optical transmittance of VO_2(M) films was recorded at wavelengths of 400−1800 nm with a variable-temperature device (Shimadzu UV3600 UV−vis−near-infrared spectrophotometer).

3. RESULTS AND DISCUSSION

3.1. Synthesis of Mo-Doped VO_2(M) Crystals. Figure 1 shows the XRD patterns of the as-prepared VO_2 powders with and without 5.62 atom % Mo doping. The strong diffraction peaks prove that both undoped and Mo-doped VO_2 are well crystallized. The diffraction peaks shown in Figure 1a can be indexed as metastable monoclinic VO_2(B) (JCPDS card no. 81-2392; space group $C2/m$) with lattice parameters a = 12.0930 Å, b = 3.7021 Å, and c = 6.4330 Å, in agreement with the reported results.[19] Figure 1b shows the diffraction peaks of the Mo-doped product, which can be indexed to monoclinic VO_2(M) (JCPDS card no. 43-1051; space group $P2_1/c$) with lattice parameters of a = 5.7517 Å, b = 4.5378 Å, and c = 5.3825 Å. It was found that the pure monoclinic Mo-doped VO_2(M) can be obtained only when the Mo doping content reaches 5.62 atom %, and the mixed phases of VO_2(B) and VO_2(M) will be obtained if the Mo doping content is lower than 5.62 atom %

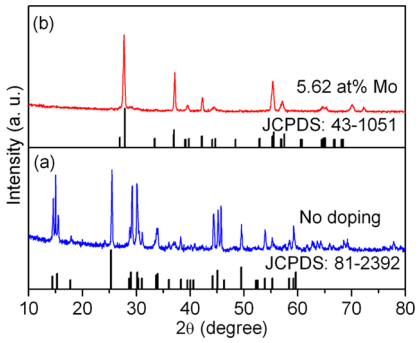

Figure 1. XRD patterns of VO_2 powders (a) without and (b) with 5.62 atom % Mo doping.

(Figure S1, Supporting Information, SI). This result demonstrates that sufficient Mo doping can promote formation of the VO_2(M) phase. Doping with Mo can induce distortion of the VO_6 octahedra by Mo atoms substituting for V atoms, making it easier to break the interconnections between different octahedra and thus reducing the activation energy of the formation of VO_2(M). Note there is a critical Mo doping content to achieve sufficient reduced activation energy of VO_2(M) formation.[7] It is worth noting that the peaks related to molybdenum oxide were not observed in Figure 1b, indicating that Mo atoms are homogeneously distributed inside the VO_2(M) crystal lattice, forming a solid solution.

Figure 2 shows FESEM images of the as-prepared VO_2 powders with and without 5.62 atom % Mo doping. It can seen

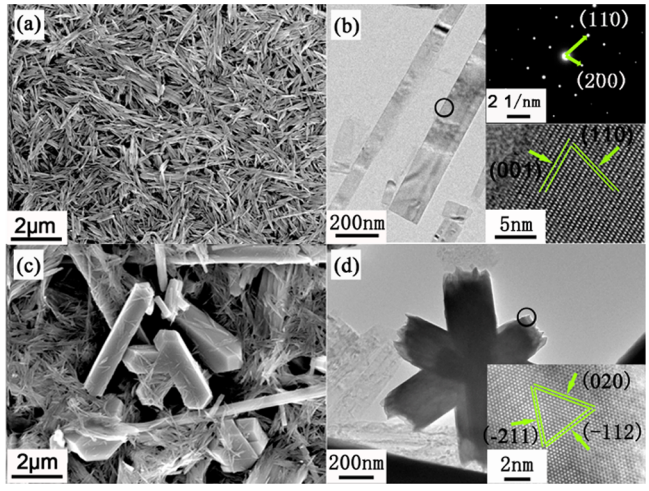

Figure 2. FESEM and TEM images of VO_2 powders without (a and b) and with (c and d) 5.62 atom % Mo doping. The insets are the corresponding SAED patterns.

from Figure 2a that VO_2(B) has a rodlike shape with lengths up to several micrometers and a typical width of 100 nm. TEM analysis (Figure 2b) confirms that the rodlike structure is formed by VO_2(B) nanorods, which is supported by the corresponding selected area electron diffraction (SAED) patterns (the upper inset in Figure 2b). The interplanar distances of 0.62 and 0.356 nm match well with the (001) and (110) crystal planes of the monoclinic VO_2(B) (the lower inset in Figure 2b). The VO_2(B) nanorods are single crystal with preferential growth along the [010] direction. With 5.62 atom % Mo doping, the asterisk-like morphology forms, as shown in Figure 2c. TEM observation (Figure 2d) shows that the asterisk

consists of VO_2(M) nanorods with a thickness of about 200 nm and a width of 300 nm. High-resolution TEM (HRTEM) analysis of the end part of an individual rod confirms that the asterisk-shaped crystals are the VO_2(M) phase. The interplanar distances of 0.228, 0.244, and 0.245 nm match well with the (020), ($\bar{1}$12), and ($\bar{2}$11) crystal planes of the monoclinic VO_2(M), which is in agreement with the XRD results and is in accordance with the previous reports.[7,20]

Figure 3 shows the DSC curves of Mo-doped VO_2(M) crystals in a typical heating cycle. One can see that the phase

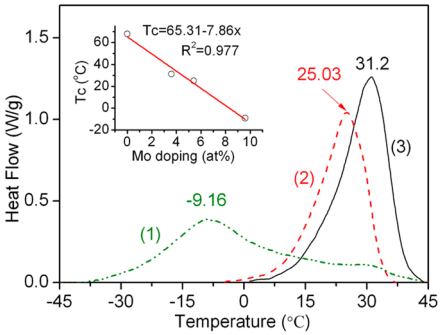

Figure 3. DSC curves of VO_2(M) powders with Mo doping contents of (1) 3.74, (2) 5.62, and (3) 9.36 atom %. The inset is a plot of T_c versus Mo doping content.

transition temperature can be reduced to room temperature with 5.62 atom % Mo doping and even to below zero with 9.36 atom % doping. This result demonstrates that Mo doping can not only promote formation of the VO_2(M) phase but effectively reduce T_c. This is slightly different from the result reported by Hanlon et al.; there they found that T_c can only be reduced to 24 °C with 7% Mo doping.[21] The inset in Figure 3 shows the relationship between the Mo doping content and T_c. An average reduction efficiency of 7.86 °C per Mo atom % can be obtained from the slope of the line:

$$T_c = 64.91 - 7.86\ \text{Mo (atom \%)} \quad (1)$$

The above results indicate that Mo-doped VO_2(M) can be fabricated via a one-step hydrothermal synthesis process, and T_c can be reduced to room temperature. Nevertheless, from Figure 2, one can see that the size of Mo-doped VO_2(M) powders is very large (in the micrometer range), which cannot meet the demands for smart window coating because of its poor dispersity and low optical transmittance. To reduce the size of the VO_2(M) crystal to the nanometer scale, it is essential to control the nucleation and growth processes of the VO_2(M) crystal in solution.

3.2. Preparation of Mo-Doped VO_2/TiO_2 Composite Nanocrystals. Figure 4 shows the XRD patterns of Mo-doped VO_2 powders with and without TiO_2 seed together with that from a physical mixing of VO_2(M) and TiO_2 nanoparticles. One can see that all observed diffraction peaks can be indexed to the monoclinic phase of VO_2(M) (JCPDS card no. 43-1051), and no noticeable diffraction peak positions changed when different TiO_2 seed contents were used (curves 2−4) but shifted slightly to a low angle when compared to the case without TiO_2 seed (curve 1). This shift could have resulted from the superposition of the diffraction peak from both rutile TiO_2 and VO_2(M) near 27.8°, as confirmed by the XRD results of the physical mixture of TiO_2 and VO_2(M) powders shown in

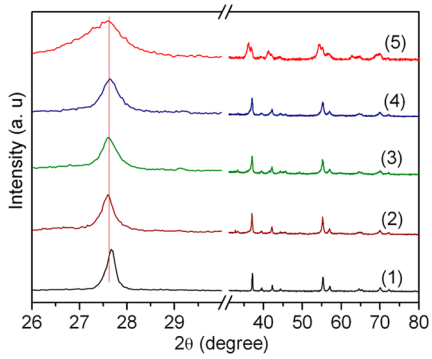

Figure 4. (a) XRD patterns of VO_2(M) powders without (1) and with TiO_2 seed of TiO_2/VO_2 molar ratios (2) 1:11, (3) 1:7, and (4) 1:5. (5) XRD pattern of a TiO_2 and VO_2 phase mixture (1:1 molar ratio).

curve 5 of Figure 4 and the Gaussian fitting results (Figure S2, SI).

Figure 5 shows the FESEM images of Mo-doped VO_2(M)/TiO_2 composite nanocrystals (with TiO_2/VO_2 molar ratios

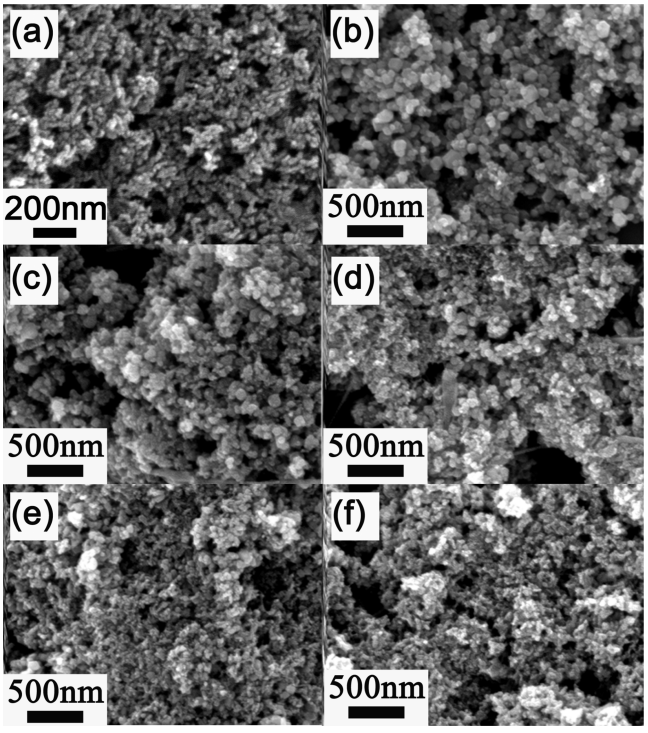

Figure 5. FESEM images of rutile TiO_2 seed (a) and Mo-doped VO_2(M)/TiO_2 composite nanocrystals with TiO_2/VO_2 molar ratios of (b) 1:11, (c) 1:9, (d) 1:7, (e) 1:5, and (f) 1:3.

from 1:11 to 1:5) together with that from TiO_2 seed. The TiO_2 seeds have uniform size distribution with an average size of 15 nm (Figure 5a). Without TiO_2 seed, the Mo-doped VO_2(M) has an asterisk-like shape (Figure 2c,d). With TiO_2 seed, all resultant Mo-doped VO_2(M)/TiO_2 composite nanocrystals possess a quasi-spherical shape. The size of the composite nanocrystals decreases with increased TiO_2 seed content and can be modulated from 100 nm (TiO_2:VO_2 = 1:11; Figure 5b) to about 20 nm (TiO_2:VO_2 = 1:5; Figure 5d). This result indicates that the introduction of TiO_2 seed can substantially reduce the size and control the morphology of VO_2(M)/TiO_2 composite nanocrystals.

dx.doi.org/10.1021/am500135d | ACS Appl. Mater. Interfaces 2014, 6, 6555−6561

Figure 6 shows the TEM and HRTEM images of Mo-doped VO_2(M)/TiO_2 composite nanocrystals (TiO_2:VO_2 = 1:11).

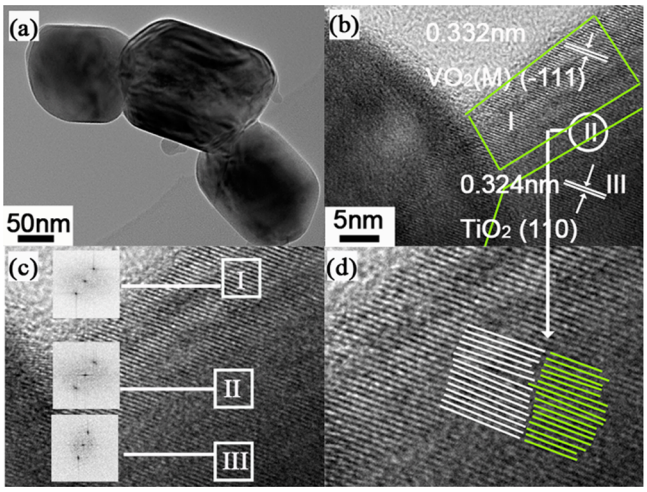

Figure 6. (a) TEM and (b and d) HRTEM images and (c) FFT patterns of Mo-doped VO_2(M)/TiO_2 composite nanocrystals with a TiO_2/VO_2 molar ratio of 1:11.

The quasi-spherical shape with a size of around 100 nm can be clearly seen in Figure 6a. The interplanar distances of 0.332 nm in area I and 0.324 nm in area II match well with the $(\bar{1}11)$ and (110) crystal planes of VO_2(M) and rutile TO_2 (Figure 6b), respectively, indicating that VO_2(M) crystals epitaxially grow on rutile TiO_2 nanocrystals, and the appearance of a dislocation in area III also confirmed epitaxial growth because of slightly different interplanar distances in VO_2(M) and TO_2. The fast Fourier transformation (FFT) patterns taken from areas I and II, as well as the transition region III shown in Figure 6c, further confirm the above results, in which the FFT spots in areas I and II are discrete because of the individual structure, while in area III, they are slightly dispersed because of the overlap of the two structures. This result reveals that rutile TiO_2 seed can lead to epitaxial growth of VO_2(M) nanocrystals.

The composition and chemical state of Mo-doped VO_2(M)/TiO_2 composite nanocrystals are investigated by XPS analysis (Figure 7). The XPS spectra were calibrated by the C 1s peak (284.6 eV) from adventurous hydrocarbon contamination on the sample surface. The survey spectrum in Figure 7a shows the existence of V, O, Mo, and Ti without any impurities. High-resolution analyses of the O 1s and V 2p peaks as well as their deconvolution based on the Gaussian function are shown in Figure 7b. One can see that the main fitting peak of V $2p_{3/2}$ is centered at 518.05 eV, which is slightly higher than that of undoped V $2p_{3/2}$ as a result of Mo doping.[22,23] The small peak at a binding energy of 516.76 eV corresponds to V^{5+} ions due to surface oxidation when exposed in air. The strong symmetrical peak at 530.88 eV can be indexed to O_{1s}. It can be seen from deconvolution of the Mo_{3d} peak (Figure 7c) that Mo is present as Mo^{6+} with binding energies of 235.61 and 232.40 eV for Mo $3d_{3/2}$ and Mo $3d_{5/2}$,[22,24] respectively, demonstrating that a Mo atom has been doped into the TiO_2/VO_2 composite. The binding energies at 459.31 and 464.93 eV are respectively attributed to the Ti $2p_{3/2}$ and Ti $2p_{1/2}$ peaks in the rutile phase TiO_2 (Figure 7d), corresponding to the position for Ti^{4+} in TiO_2, and are slightly higher than that in pure TiO_2 (the reported value for pure Ti is 458.0−458.5 eV[25]). The increase

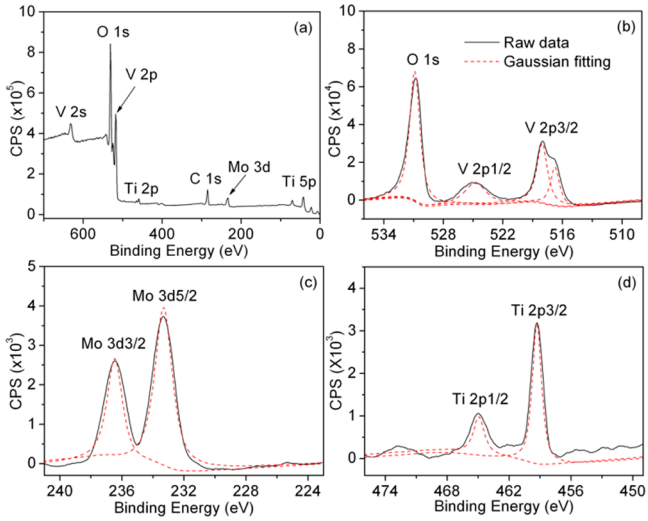

Figure 7. XPS spectra of Mo-doped VO_2(M)/TiO_2 composite nanocrystals with a TiO_2/VO_2 molar ratio of 1:11: (a) survey spectral high-resolution scan of (b) V 2p, O 1s, (c) Mo 3d, and (d) Ti 2p and the corresponding Gaussian fittings.

in the binding energy might be due to electronic interactions between Ti and the doped Mo.[25]

Figure 8 shows the DSC curves of 5.62 atom % Mo-doped VO_2(M) nanocrystals without and with TiO_2 seed (TiO_2/VO_2

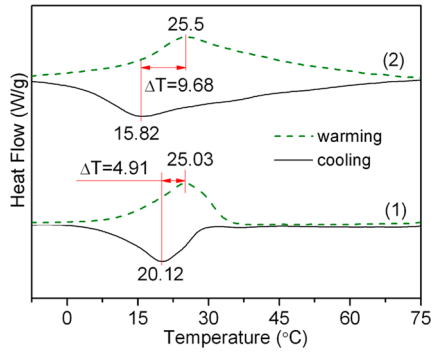

Figure 8. DSC curves of Mo-doped VO_2(M) nanocrystals without (1) and with (2) TiO_2 seed (TiO_2/VO_2 molar ratio of 1:11).

molar ratio of 1:11). The endothermic and exothermic peaks in each DSC curve can be clearly seen, which further confirms the formation of VO_2(M) in a one-step hydrothermal synthesis and is in agreement with the XRD result. The peak temperature in the heating cycle is slightly increased from 25.03 °C without seed to 25.5 °C with seed, while it decreases from 20.12 °C without seed to 15.82 °C with seed in the cooling cycle. The calculated latent heat from Figure 8 in the heating cycle is 31.5 and 11.7 J/g for Mo-doped VO_2(M) nanocrystals with and without TiO_2 seed. The higher latent heat indicates that Mo-doped VO_2(M)/TiO_2 composite nanocrystals are highly crystalline and relatively perfect in their crystalline structure.[26] Hysteresis between the heating and cooling cycles increases with TiO_2 seed (from 4.91 to 9.68 °C), which is different from the reported result that TiO_2 additives can remarkably reduce the hysteresis loop width,[18] and is considered to be due to the size effect of Mo-doped VO_2(M)/TiO_2 composite nanocrystals.[27,28]

dx.doi.org/10.1021/am500135d | ACS Appl. Mater. Interfaces 2014, 6, 6555−6561

Figure 9 shows the DSC curves of 5.62 atom % Mo-doped VO_2(M)/TiO_2 composite nanocrystals with different TiO_2 seed

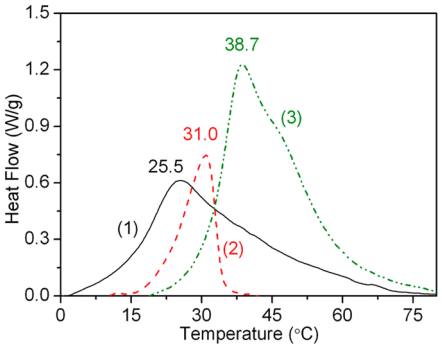

Figure 9. DSC curves of Mo-doped VO_2(M)/TiO_2 composite nanocrystals with TiO_2/VO_2 molar ratios of (1) 1:11, (2) 1:7, and (3) 1:5.

contents in the heating cycle. One can see that the peak temperature increases with increasing TiO_2 seed content despite having the same Mo doping content (e.g., T_c increases from 25.50 to 38.72 °C when the TiO_2/VO_2 molar ratio increases from 1:11 to 1:5). This result indicates that the addition of TiO_2 seed suppresses the Mo doping content in VO_2(M). Table 1 shows the influence of the TiO_2 seed content

Table 1. Influence of TiO_2 Seed on the Phase Transition Temperature and Mo Doping Content in VO_2(M) Crystals

TiO_2/VO_2 molar ratio	T_c by DSC (°C)	Mo doping by XPS (atom %)	Ti/V by XPS (atom %)	calcd Mo doping (atom %)
0	25.03	9.26	/	5.125
1:11	25.50	10.23	1:18	5.065
1:7	31.04	9.44	1:11	4.360
1:5	38.72	9.96	1:10	3.383

on T_c and the Mo doping content calculated from formula (1) and by XPS analysis. It was found that the Mo doping content detected by XPS almost has a constant value and is very large compared to the target Mo doping content (5.62 atom %), while the Ti/V ratio by XPS increases with increasing TiO_2 seed content because XPS is a surface-sensitive technique, probing only the first few atomic layers. The fact that the Mo doping content detected by XPS is larger than the target doping content indicates that surface Mo enrichment has occurred. On the other hand, the fact that the actual Mo doping content calculated from formula (1) in the last column of Table 1 decreases with increasing TiO_2 seed content might also indicate that not all Mo is doped in VO_2(M) (because the phase transition temperature increases with increasing TiO_2 content) but exists in other forms such as doped into TiO_2[24,29] or in a separate Mo_2O_3 phase.

Figure 10 shows variable-temperature (from −40 to +80 °C) optical transmittance in the visible-light and near-infrared regions of Mo-doped VO_2(M) composite nanocrystal thin films. One can see that infrared transmittance only changes about 10% (Figure 10a) before and after phase transition for 5.62 atom % Mo-doped VO_2(M) (T_c = 25.03 °C) without TiO_2 seed. The infrared modulation is substantially enhanced with TiO_2 seed and increases with increasing TiO_2 seed content. The infrared modulation increases to about 23%

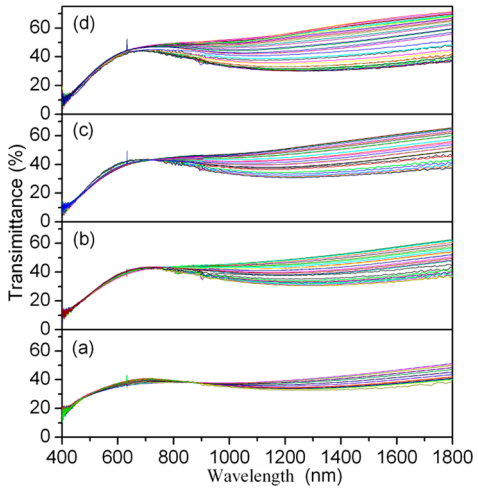

Figure 10. Variable-temperature transmission spectra of a Mo-doped VO_2(M) crystal film without TiO_2 seed (a) and with TiO_2/VO_2 molar ratios of (b) 1:11, (c) 1:7, and (d) 1:5.

(Figure 10b) with a TiO_2/VO_2 molar ratio of 1:11 (T_c = 25.50 °C) and further increases to 35% (Figure 10d) with a TiO_2/VO_2 molar ratio of 1:5 (T_c = 38.72 °C). Transmittance in the visible-light region also slightly increases with TiO_2 seed, which is inconsistent with the literature reports.[18,30,31] The hysteresis loop at 1500 nm of Mo-doped TiO_2/VO_2 (M) composite nanocrystal thin films [hysteresis width between 70 and 82 °C with VO_2(M) sizes of 100, 60, and 20 nm; Figures S3b−d, SI] is larger than that for a Mo-doped VO_2(M) crystal thin film [hysteresis width of about 50 °C with VO_2(M) size between 200 and 300 nm; Figure S3a, SI] due to the size effect, which is inconsistent with the DSC result shown in Figure 8. A high solar modulation ability is very important for the application of VO_2(M) as smart windows,[32,33] and further work is underway to study the thermochromic performance of the Mo-doped TiO_2/VO_2(M) composite nanocrystal film on a glass substrate.

3.3. TiO_2 Seed Growth Mechanism. The growth of VO_2(R) on TiO_2 seed may be described in accordance with the nucleation−growth mechanism. Without TiO_2 seed, the growth of VO_2(M) crystals has to overcome nucleation energy (ΔG_r) and surface free energy (ΔG_s). So, the free energy needed for the formation of VO_2(R) crystals can be expressed by the following equations:

$$\Delta G = \Delta G_r + \Delta G_s \quad (2)$$

$$\Delta G_s = 4\pi r^2 \gamma \quad (3)$$

where γ denotes the surface tension of VO_2(R) grain. Because the lattice parameters of VO_2(R) and rutile TiO_2 are very similar, the surface tension γ is also nearly the same as that of TiO_2 seed; therefore, the growth of VO_2(R) on TiO_2 seed only needs to overcome the nucleation energy ($\Delta G_s \approx \Delta G_r$) and thus facilitates the nucleation and growth of VO_2(R) grain. From the perspective of crystal growth kinetics, it is easy to understand that the higher the seed content, the smaller the epitaxial crystals because of the limited VO_2(R) raw material; thus, the size of Mo-doped VO_2(M)/TiO_2 composite nanocrystals decreases with increasing TiO_2 seed content.

4. CONCLUSION

In summary, Mo-doped VO_2(M)/TiO_2 composite nanocrystals have been fabricated by a one-step hydrothermal synthesis

method. The morphology changes from asterisk-like shape with size in the micrometer range for Mo-doped VO_2(M) without TiO_2 seed to quasi-spherical shape with size down to 20 nm for Mo-doped VO_2(M)/TiO_2 composite nanocrystals with TiO_2 seed. The size of the composite nanocrystals decreases with increasing TiO_2 seed content, and the phase transition temperature can be modulated to room temperature. The infrared modulation can be substantially enhanced with the addition of TiO_2 seed, and nearly 35% modulation can be realized. The findings of this work not only provided a simple means to achieve control of the morphology and size of VO_2(M) nanocrystals but also demonstrated that the infrared modulation can be enhanced by the addition of TiO_2 nanocrystals.

■ ASSOCIATED CONTENT

Supporting Information

Data of Gaussian fitting results of the XRD peak near 27.8° for Mo-doped VO_2(M) crystals with and without TiO_2 seed, XRD pattern and FESEM image of a Mo-doped VO_2(M) crystal with a Mo doping content of 3.74 atom %, and hysteresis loop at 1500 nm of a Mo-doped VO_2(M) crystal film with and without TiO_2 seed. This material is available free of charge via the Internet at http://pubs.acs.org.

■ AUTHOR INFORMATION

Corresponding Author

*E-mail: ghli@issp.ac.cn.

Notes

The authors declare no competing financial interest.

■ ACKNOWLEDGMENTS

The authors thank Prof. Huijun Zhao at the Center for Clean Environment and Energy, Griffith University, Nathan, Australia, for useful discussions. This work was financially supported by the National Natural Science Foundation of China (Grants 51372250 and 11104270) and the National Basic Research Program of China (Grant 2009CB939903).

■ REFERENCES

(1) Morin, F. J. Oxides which Show a Metal-to-Insulator Transition at the Neel Temperature. *Phys. Rev. Lett.* **1959**, *3*, 34−36.

(2) Park, J. H.; Coy, J. M.; Kasirga, S.; Huang, C.; Fei, Z.; Hunter, S.; Cobden, D. H. Measurement of a Solid-State Triple Point at the Metal−Insulator Transition in VO_2. *Nature* **2013**, *500*, 431−434.

(3) Case, F. C. Improved VO_2 Thin Films for Infrared Switching. *Appl. Opt.* **1991**, *30*, 4119−4123.

(4) Livage, J.; Guzman, G.; Beteille, F. Optical Properties of Sol−Gel Derived Vanadium Oxide Films. *J. Sol−Gel Sci. Technol.* **1997**, *8*, 857−865.

(5) Beteille, F.; Livage, J. Optical Switching in VO_2 Thin Films. *J. Sol−Gel Sci. Technol.* **1998**, *13*, 915−921.

(6) Goodenough, J. B. The Two Components of the Crystallographic Transition in VO_2. *J. Solid State Chem.* **1971**, *3*, 490−500.

(7) Cao, C.; Gao, Y.; Luo, H. Pure Single-Crystal Rutile Vanadium Dioxide Powders: Synthesis, Mechanism and Phase-Transformation Property. *J. Phys. Chem. C* **2008**, *112*, 18810−18814.

(8) Ji, S.; Zhao, Y.; Zhang, F.; Jin, P. Direct Formation of Single Crystal VO_2(R) Nanorods by One-step Hydrothermal Treatment. *J. Cryst. Growth* **2010**, *312*, 282−286.

(9) Son, J. H.; Wei, J.; Cobden, D.; Cao, G.; Xia, Y. Hydrothermal Synthesis of Monoclinic VO_2 Micro- and Nanocrystals in One Step and Their Use in Fabricating Inverse Opals. *Chem. Mater.* **2010**, *22*, 3043−3050.

(10) Whittaker, L.; Jaye, C.; Fu, Z.; Fischer, D. A.; Banerjee, S. Depressed Phase Transition in Solution-Grown VO_2 Nanostructures. *J. Am. Chem. Soc.* **2009**, *131*, 8884−8894.

(11) Whittaker, L.; Wu, T. L.; Patridge, C. J.; Sambandamurthy, G.; Banerjee, S. Distinctive Finite Size Effects on the Phase Diagram and Metal-Insulator Transitions of Tungsten-doped Vanadium(IV) Oxide. *J. Mater. Chem.* **2011**, *21*, 5580−5592.

(12) Wu, C.; Feng, F.; Feng, J.; Dai, J.; Yang, J.; Xie, Y. Ultrafast Solid-state Transformation Pathway from New-Phased Goethite VOOH to Paramontroseite VO_2 to Rutile VO_2(R). *J. Phys. Chem. C* **2011**, *115*, 791−799.

(13) Yao, T.; Liu, L.; Xiao, C.; Zhang, X.; Liu, Q.; Wei, S.; Xie, Y. Ultrathin Nanosheets of Half-Metallic Monoclinic Vanadium Dioxide with a Thermally Induced Phase Transition. *Angew. Chem., Int. Ed.* **2010**, *52*, 7554−7558.

(14) Wu, C.; Dai, J.; Zhang, X.; Yang, J.; Qi, F.; Gao, C.; Xie, Y. Direct Confined-Space Combustion Forming Monoclinic Vanadium Dioxides. *Angew. Chem., Int. Ed.* **2010**, *49*, 134−137.

(15) Wilkinson, M.; Kafizas, A.; Bawaked, S. M.; Obaid, A. Y.; Al-Thaiti, S. A.; Basahel, S. N.; Carmalt, C. J.; Parkin, I. P. Combinatorial Atmospheric Pressure Chemical Vapor Deposition of Graded TiO_2−VO_2 Mixed-Phase Composites and Their Dual Functional Property as Self-Cleaning and Photochromic Window Coating. *ACS Comb. Sci.* **2013**, *15*, 309−319.

(16) Mlyuka, N. R.; Niklasson, G. A.; Granqvist, C. G. Thermochromic Multilayer Films of VO_2 and TiO_2 with Enhanced Transmittance. *Sol. Energy Mater. Sol. Cells* **2009**, *93*, 1685−1687.

(17) Jin, P.; Xu, G.; Tazawa, M.; Yoshimura, K. Design, Formation and Characterization of a Novel Multifunctional Window with VO_2 and TiO_2 Coatings. *Appl. Phys. A: Mater. Sci. Process.* **2003**, *77*, 455−459.

(18) Li, Y.; Ji, S.; Gao, Y.; Luo, H.; Kanehira, M. Core−Shell VO_2@TiO_2 Nanorods That Combine Thermochromic and Photocatalytic Properties for Application as Energy-Saving Smart Coatings. *Sci. Rep.* **2013**, *3*, 1370.

(19) Li, M.; Kong, F.; Zhang, Y.; Li, G. Hydrothermal Synthesis of VO_2(B) Nanorings with Inorganic V_2O_5 Sol. *CrystEngComm* **2011**, *13*, 2204−2207.

(20) Li, M.; Li, D. B.; Pan, J.; Lin, J. C.; Li, G. H. Selective Synthesis of Vanadium Oxides and Investigation of the Thermochromic Properties of VO_2 by Infrared Spectroscopy. *Eur. J. Inorg. Chem.* **2013**, *2013*, 1207−1212.

(21) Batista, C.; Teixeira, V.; Ribeiro, R. M. Synthesis and Characterization of $V_{1-x}Mo_xO_2$ Thermochromic Coatings with Reduced Transition Temperatures. *J. Nanosci. Nanotechnol.* **2010**, *10*, 1393−1397.

(22) Yan, J.; Zhang, Y.; Huang, W.; Tu, M. Effect of Mo−W Co-doping on Semiconductor−Metal Phase Transition Temperature of Vanadium Dioxide Film. *Thin Solid Films* **2008**, *516*, 8554−8558.

(23) Sun, Y.; Jiang, S.; Bi, W.; Long, R.; Tan, X.; Wu, C.; Wei, S.; Xie, Y. New Aspects of Size-Dependent Metal-Insulator Transition in Synthetic Single-Domain Monoclinic Vanadium Dioxide Nanocrystals. *Nanoscale* **2011**, *3*, 4394−4404.

(24) Shen, Y.; Xiong, T.; Du, H.; Jin, H.; Shang, J.; Yang, K. Phosphorous, Nitrogen, and Molybdenum Ternary Co-doped TiO_2: Preparation and Photocatalytic Activities under Visible Light. *J. Sol−Gel Sci. Technol.* **2009**, *50*, 98−102.

(25) Reddy, B. M.; Chowdhury, B.; Smirniotis, P. G. An XPS Study of the Dispersion of MoO_3 onTiO_2−ZrO_2, TiO_2−SiO_2, TiO_2−Al_2O_3, SiO_2−ZrO_2, and SiO_2−TiO_2−ZrO_2 Mixed Oxides. *Appl. Catal., A* **2001**, *211*, 19−30.

(26) Chen, Z.; Gao, Y. F.; Kang, L. T.; Cao, C. X.; Chen, S.; Luo, H. Fine Crystalline VO_2 Nanoparticles: Synthesis, Abnormal Phase Transition Temperatures and Excellent Optical Properties of a Derived VO_2 Nanocomposite Foil. *J. Mater. Chem. A* **2014**, *2*, 2718−2727.

(27) Suh, J. Y.; Lopez, R.; Feldman, L. C.; Haglund, R. F. Semiconductor to Metal Phase Transition in the Nucleation and

Growth of VO_2 Nanoparticles and Thin Films. *J. Appl. Phys.* **2004**, *96*, 1209−1212.
(28) Dai, L.; Cao, C.; Gao, Y.; Luo, H. Synthesis and Phase Transition Behavior of Undoped VO_2 with a Strong Nano-size Effect. *Sol. Energy Mater. Sol. Cells* **2011**, *95*, 712−715.
(29) Devi, L. G.; Murthy, B. N. Characterization of Mo Doped TiO_2 and its Enhanced Photo Catalytic Activity Under Visible Light. *Catal. Lett.* **2008**, *125*, 320−330.
(30) Verleur, H. W.; Barker, A. S., Jr.; Berglund, C. N. Optical Properties of VO_2 between 0.25 and 5 eV. *Phys. Rev. Lett.* **1968**, *172*, 788−798.
(31) Zhang, Z.; Gao, Y.; Kang, L.; Du, J.; Luo, H. Effects of a TiO_2 Buffer Layer on Solution-Deposited VO_2 Films: Enhanced Oxidization Durability. *J. Phys. Chem. C* **2010**, *114*, 22214−22220.
(32) Kang, L.; Gao, Y.; Luo, H.; Chen, Z.; Du, J.; Zhang, Z. Nanoporous Thermochromic VO_2 Films with Low Optical Constants, Enhanced Luminous Transmittance and Thermochromic Properties. *ACS Appl. Mater. Interfaces* **2011**, *3*, 135−138.
(33) Gao, Y.; Cao, C.; Dai, L.; Luo, H.; Kanehira, M.; Ding, Y.; Wang, Z. Phase and Shape Controlled VO_2 Nanostructures by Antimony Doping. *Energy Environ. Sci.* **2012**, *5*, 8708−8715.